KEK Preprint 94-187
January 1995
M/R

Compton Scattering of 20- to 40-keV Photons

Y. NAMITO, S. BAN, H. HIRAYAMA, N. NARIYAMA, H. NAKASHIMA,
Y. NAKANE, Y. SAKAMOTO, N. SASAMOTO.
Y. ASANO and S. TANAKA

To be published in Phys. Rev. A.

National Laboratory for High Energy Physics, 1995

KEK Reports are available from:

Technical Information & Library
National Laboratory for High Energy Physics
1-1 Oho, Tsukuba-shi
Ibaraki-ken, 305
JAPAN

Phone: 0298-64-1171
Telex: 3652-534 (Domestic)
(0)3652-534 (International)
Fax: 0298-64-4604
Cable: KEK OHO
E-mail: LIBRARY@JPNKEKVX (Bitnet Address)
library@kekvax.kek.jp (Internet Address)

Compton Scattering of 20- to 40-keV Photons

Y. Namito, S. Ban, and H. Hirayama
National Laboratory for High Energy Physics Oho, Tsukuba-shi, Ibaraki-ken, 305, Japan

N. Nariyama
Ship Research Institute, Shinkawa, Mitaka-shi, Tokyo-to, 181, Japan

H. Nakashima, Y. Nakane, Y. Sakamoto, N. Sasamoto, Y. Asano and S. Tanaka
Japan Atomic Energy Research Institute, Tokai-mura, Ibaraki-ken, 319-11, Japan
(January 23, 1995)

The scattered-energy spectra of monochronized synchrotron-radiation photons toward 90° by C, Al, Fe, Cu, Au and Pb samples were measured using high-purity Ge detectors to obtain incoherent scattering function (S) in the $1.14 < x < 2.28$ Å^{-1} region. The multiple-scattering intensity was evaluated by a Monte-Carlo calculation while considering the Doppler broadening of the Compton-scattered photons and the photon linear polarization. The measured S of C, Al, Fe and Cu agreed with that based on the Waller-Hartree theory (S^{WH}) as well as that based on a relativistic impulse approximation (S^{IA}) within the experiment error (2.5%). The measured S of high-Z atoms (Au and Pb) agrees with S^{IA}, and is smaller than S^{WH} by 3 to 6%.

32.80.Cy

I. INTRODUCTION

The Compton-scattering cross section of a free electron is described by the well-known Klein-Nishina formula [1]. In the case that the electron binding effect is not negligible, Compton scattering must be treated as scattering by a bound electron. The incoherent scattering function ($S(x,Z)$) is defined as the ratio of the differential Compton-scattering cross sections of bound electrons in one whole atom ($(\frac{d\sigma}{d\Omega})_{bC}$) and one free electron ($(\frac{d\sigma}{d\Omega})_{fC}$),

$$S(x,Z) = (\frac{d\sigma}{d\Omega})_{bC} / (\frac{d\sigma}{d\Omega})_{fC}, \tag{1}$$

where

$$(\frac{d\sigma}{d\Omega})_{fC} = (\frac{r_0^2}{2})(\frac{k_c}{k_0})^2(\frac{k_c}{k_0} + \frac{k_0}{k_c} - \sin^2\theta), \tag{2}$$

$$k_c = \frac{k_0}{1 + \frac{k_0}{m_0c^2}(1 - \cos\theta)}, \tag{3}$$

and

$$x = \frac{k_0}{12.399} \sin(\frac{\theta}{2}). \tag{4}$$

Here, r_0 is the classical electron radius, k_0 and k_c are the incident and Compton-scattered photon energies for an electron at rest in keV , θ is the scattering polar angle and Z is the atomic number of the atoms in the scatterer; x is the momentum transfer in Å^{-1}. While S is usually treated as a function of x and Z, it is also treated as a function of k_0, θ and Z.

Theoretical values of an incoherent-scattering function based on the Waller-Hartree theory [2] (S^{WH}) is widely used for keV photon-transport calculations [3–7]. It is also possible to calculate the incoherent scattering function by integrating the double differential Compton-scattering cross section based on an impulse approximation with respect to the scattered photon energy (S^{IA}) [8,9].

Three groups performed systematic measurements of the incoherent scattering function over a wide range of momentum transfer using a Ge(Li) detector. The incoherent scattering function of Al, Cu, Mo,

Sn, Ta, Pb was measured by Dow et al. [10] within the $1.21 < x < 14.8$ Å^{-1} region. Measurements of the incoherent-scattering function of Cu, Sn and Pb within the $3.7 < x < 11.3$ Å^{-1} region was made by Kane et al. [11,12]. The incoherent scattering function of Cu, Zn, Cd, Sn, W, Pt, Pb and U for $2.3 < x < 27$ Å^{-1}, measured by Goncalves et al. [13], has a relatively large estimated error compared to Dow's and Kane's measurements.

Incoherent-scattering function measurements using a scintillation detector were performed [14–21]. However, the error of the incoherent-scattering function measured using a scintillation counter was large, because it is difficult to separate Rayleigh-scattered photons from incoherent-scattering photons in the $x \lesssim 2$ Å^{-1} region where the electron binding effect is evident.

Several incoherent-scattering function measurements were carried out in a low momentum-transfer region ($x \lesssim 1$ Å^{-1}). Measurements of the incoherent-scattering function of Be, Al, LiF, Li and Na were perfomed by Phillips and Weiss [22]; and Si and Ge incoherent-scattering function measurements were performed by Paakkari and Suortti [23]. The incoherent-scattering function of Al in the $0.3 < x < 0.6$ Å^{-1} region was measured by Walker [24]. The incoherent-scattering function of C was measured in the $x < 0.4$ Å^{-1} region by Laval [25]. Kahane measured the incoherent scattering function of Cu in the $0.6 < x < 2.0$ Å^{-1} region using neutron capture gamma rays [26].

Measurements of the incoherent-scattering function conducted before 1975 have been summarized by Hubbell et al. [27]. Kane summarized the inelastic scattering of x-rays and gamma rays by inner shell electrons [28].

In this study, the differential Compton-scattering cross section of 20- to 40-keV photons for C, Al, Fe, Cu, Au and Pb toward 90° direction was measured using high-purity Ge detectors so as to obtain an incoherent-scattering function in the $1.1 < x < 2.3$ Å^{-1} region. A monochronized synchrotron-radiation photon beam was used in the measurement. The main features of the synchrotron-radiation photons are brightness, mono-directional propagation and energy tunability. Utilizing these features, measurements were performed in a good geometry with a narrow angular spread.

One feature of this measurement is a clear separation of Rayleigh scattering from Compton scattering. This separation is important for measuring the Compton-scattering intensity with a small error, because, if not separated clearly Rayleigh scattering is a serious source of error in incoherent-scattering function measurements. This is because the Rayleigh-scattering intensity is of the same order as that of Compton scattering, and the Rayleigh-scattering intensity fluctuates depending on the condition of the sample. The energy difference of Rayleigh and Compton scattering is small in the small momentum-transfer region. It depends on x, and is almost independent of the incident photon energy, as long as x maintains a constant value. For example, $x = 2.281$ Å^{-1} is obtained by using a combination of $k_0 = 40.0$keV and $\theta = 90°$ or $k_0 = 662$keV and $\theta = 4.9°$; the energy differences of Rayleigh- and Compton- scattered photons are 2.9 and 3.1keV in each combination. In this measurement, the energy difference of Rayleigh and Compton scattering was sufficiently large compared with the energy resolution of the detectors (FWHM $\simeq$ 0.3keV), since the combination of a low incident energy($20 - 40$keV) and a wide scattering angle(90°) was used. As a result, the Rayleigh-scattered photons were separated clearly.

Another feature of this study was a Monte-Carlo estimation of multiple-scattering photons. Thick samples were used to reduce the influence of the sample thickness fluctuation. While the fluctuation of the Compton-scattering intensity due to the error of the sample thickness was negligible, the multiple-scattering intensity increased up to 10% as a trade off. Thus the multiple-scattering intensity was evaluated by a Monte-Carlo calculation, and was subtracted from the measured Compton-scattering photons.

II. EXPERIMENTAL DETAILS

Measurements were performed at BL-14C in a 2.5-GeV synchrotron-light facility (KEK-PF). The experimental arrangement is shown in fig. 1. Photons from a vertical wiggler were used after being monochronized by a Si(1,1,1) double-crystal monochromator. The incident beams were 20, 25, 30, 35 and 40keV linearly polarized photons. In fig. 1, the propagation and polarization vectors of an incident photon are shown as $\vec{k_0}$ and $\vec{e_0}$. Incident photons passed through a collimator (C_0) with an opening diameter(D_0) of 2mm and a free air ionization chamber (FAIC), and were scattered by the sample (S). The photon intensity was monitored by the FAIC, which was calibrated by a calorimeter [29].

A list of the samples and their thicknesses is given in Tabel I. The normal vector of the samples was set as $(-\frac{1}{2}, -\frac{1}{\sqrt{2}}, \frac{1}{2})$. The effective thicknesses for incident photons of the Fe, Cu, Au and Pb samples were more than 10 mean-free-paths for all of the photon energies used; these samples were treated as infinitely

thick samples. The samples were contained in a vacuum chamber, and vacuum pipes were placed between the vacuum chamber and the Ge detectors in order to reduce any scattering due to air.

Photons through collimators (C_1 and C_2) located in the X and Y directions were detected by Ge detectors (Ge-1 and Ge-2). The distances from the surface of the sample to the exits of the collimators (L_1 and L_2) were 424 and 436 mm, respectively, and the opening diameters of the collimators (D_1 and D_2) were 5.01 and 5.04 mm, respectively. The scattered photon intensity had an azimuth angle dependence, since the incident photon beam comprized linearly polarized photons. To compensate for the effect of linear polarization, the scattered-photon intensity was measured by two Ge detectors located in two different azimuth-angle directions. Two high-purity Ge low-energy-photon detectors (ORTEC GLP16195/10 and GLP16195/10P) were used for the measurement. The full energy response of these detectors for photons, estimated by a Monte-Carlo calculation using the EGS4 code [30], is shown in fig.2. The difference in the responses of the two detectors was due to different Be-window thicknesses.

The signal from the detector was amplified by an ORTEC 572 amplifier, passed through a 1850-ADC(Seiko EG&G) and stored in 4k-memory in a Model-7800 multichannel analyzer (Seiko EG&G). The measurements were repeated 5 times on the average. The typical accumulation time was 600 sec.

III. DATA ANALYSIS

Based on the measured number of scattered photons ($n_x(k)$ and $n_y(k)$), the single Compton-scattering intensities toward the x and y directions (C_x and C_y) were derived as

$$C_x(k) = \frac{1}{\Omega_x \eta_x(k)}\Big(\frac{n_x(k)}{I_0} - \frac{n_x^{bg}(k)}{I_0^{bg}} - n_x^{ms}(k)\Big), \tag{5a}$$

$$C_y(k) = \frac{1}{\Omega_y \eta_y(k)}\Big(\frac{n_y(k)}{I_0} - \frac{n_y^{bg}(k)}{I_0^{bg}} - n_y^{ms}(k)\Big). \tag{5b}$$

Here, k is the scattered photon energy, Ω_x and Ω_y are the opening solid angles of the collimators, η_x and η_y are the full-energy peak efficiencies of the Ge detectors (Fig.2), and n_x^{bg} and n_y^{bg} are the background counts obtained from a no-sample run. The background count was negligibly small (< 0.2% of sample run). I_0 and I_0^{bg} are the number of incident photons during a sample run and a no-sample run. $n_x^{ms}(k)$ and $n_y^{ms}(k)$ are the multiple-scattering intensity and the single Rayleigh-scattering intensity toward the X and Y directions. The multiple-scattering intensity and the single Rayleigh-scattering intensity were evaluated using the Monte-Carlo code EGS4 while considering linearly-polarized photon scattering [31] and the Doppler broadening of a Compton-scattered photon [32], and smeared by a Gaussian function so as to account for the resolution of the Ge detectors. A dead-time correction was made using the ratio of the live time and the real time of ADC; a pile-up correction was made using the count ratio of the pile-up part and the Compton and Rayleigh-scattering parts of the measured spectrum. The dead time was controlled to be less than 2%, and the pile up was controlled to be less than 1%. Corrections for the attenuation due to the ~10cm air path between the FAIC and the vacuum chamber and a few cm air path between vacuum pipe and the Be window of the Ge detectors, as well as attenuation due to the 25 μm Kapton film at the entrance and exit of the vacuum case were also made.

On the other hand, the probability of a single Compton scattering of a photon by a plane scatterer is calculated as

$$C_x(k) = G(\theta_2 = \theta_2^x) \times \Big\{\Big(\frac{d^2\sigma}{d\Omega dk}(\phi = 0)\Big)\frac{S_0 + S_1}{2S_0} + \Big(\frac{d^2\sigma}{d\Omega dk}(\phi = \frac{\pi}{2})\Big)\frac{S_0 - S_1}{2S_0}\Big\}, \tag{6a}$$

$$C_y(k) = G(\theta_2 = \theta_2^y) \times \Big\{\Big(\frac{d^2\sigma}{d\Omega dk}(\phi = 0)\Big)\frac{S_0 - S_1}{2S_0} + \Big(\frac{d^2\sigma}{d\Omega dk}(\phi = \frac{\pi}{2})\Big)\frac{S_0 + S_1}{2S_0}\Big\}, \tag{6b}$$

where

$$G = \frac{1}{\mu(k_0) + \frac{\cos\theta_1}{\cos\theta_2}\mu(k)}\frac{N_0\rho}{A}\Big[1 - exp\Big\{-\Big(\frac{\mu(k_0)}{\cos\theta_1} + \frac{\mu(k)}{\cos\theta_2}\Big)t\Big\}\Big], \tag{7}$$

$$\frac{d^2\sigma}{d\Omega dk} = \sum_i N_i\Big(\frac{d^2\sigma}{d\Omega dk}\Big)_{bC\cdot i}, \tag{8}$$

$$\left(\frac{d^2\sigma}{d\Omega dk}\right)_{bC\cdot i} = \frac{r_0^2}{2}\frac{k}{k_0}\frac{1}{|\vec{k_0}-\vec{k}| - (k_0-k)\frac{p_z}{137}}\left(\frac{k_c}{k_0}+\frac{k_0}{k_c}-2\sin^2\theta\cos^2\phi\right)J_i(p_z), \tag{9}$$

$$p_z = -137\frac{k_0 - k - k_0k(1-\cos\theta)/m_0c^2}{|\vec{k_0}-\vec{k}|}, \tag{10}$$

and

$$|\vec{k_0}-\vec{k}| = \sqrt{k_0^2+k^2-2k_0k\cos\theta}. \tag{11}$$

Here, S_0 and S_1 are the Stoke's parameter used to represent the degree of incident polarization; θ_1 and θ_2 are the angles of incident propagation and the normal vector of the sample, scattered propagation vector and normal vector of the sample, respectively (See fig.3); $\cos\theta_1 = 1/2$, $\cos\theta_2^x = 1/2$ and $cos\theta_2^y = 1/\sqrt{2}$; ϕ is the scattering azimuth angle. $\mu(k_0)$ and $\mu(k)$ are the total attenuation coefficient of the incident and scattered photons in the sample. The values of μ were taken from the PHOTOX library [33]. N_0 is Avogadro's number, ρ and A are the density and atomic weight of the sample and t is the sample thickness; i denotes the subshell number and N_i is the number of electrons in the i-th subshell; p_z is the projection of the electron pre-collision momentum on the photon-scattering vector in atomic units, $J_i(p_z)$ is the Compton profile of an electron in the i-th subshell [34] and m_0c^2 is the electron rest mass. Eq.(9) is a double-differential Compton-scattering cross-section formula in the relativistic impulse approximation derived by Ribberfors [35,36].

In fig.4, the scattered-photon spectrum from a Pb sample is shown as an example (k_0=40keV). The average of the values in the X and Y directions is given. The measured and calculated values (sum of the single- and multiple-scattering intensity) are shown in symbols and the solid line, respectively. The sharp peak at 30keV is the Ge K X-ray escape peak of the Rayleigh-scattering peak at 40keV. The broad peak at 37keV is the Compton-scattering peak. The Compton- and Rayleigh-scattering peaks are clearly separated. The multiple-scattering and Rayleigh-scattering photon intensity evaluated by an EGS4 Monte-Carlo calculation is also indicated as the dashed line in fig.4. The ratio of the multiple-scattering photon intensity is 8% in the Compton scattering peak region in this case.

By adding $C_x(k)/G(\theta_2=\theta_2^x)$ and $C_y(k)/G(\theta_2=\theta_2^y)$, the Stokes parameter disappears,

$$\begin{aligned}\frac{C_x(k)}{G(\theta_2=\theta_2^x)}+\frac{C_y(k)}{G(\theta_2=\theta_2^y)} &= \frac{d^2\sigma}{d\Omega dk}(\phi=0)+\frac{d^2\sigma}{d\Omega dk}(\phi=\frac{\pi}{2}) \\ &= \frac{d^2\sigma}{d\Omega dk}(\phi=\frac{\pi}{4}).\end{aligned} \tag{12}$$

After being smeared by a Gaussian function in order to account for the resolution of the Ge detectors, $\frac{d^2\sigma}{d\Omega dk}(\phi=\pi/4)$ was fitted to the experimental values shown as the left-hand side of eq.12 by the least-squares method. The incoherent-scattering function (S) was obtained by integrating the fitted $\frac{d^2\sigma}{d\Omega dk}(\phi=\pi/4)$. In fig.5, the result of the fitting is shown as an example. The sample was Pb with k_0=40keV.

A list of the possible errors and their magnitudes is given in Table II. The total amount of the error was estimated to be 2.5%. The biggest source of the error is the uncertainty in the total attenuation coefficient.

IV. RESULTS

In figs.6 (a) to (f), the measured value of the incoherent scattering function (S) of C, Al, Fe, Cu, Au and Pb are shown along with previous measurements and theoretical values based on Waller-Hartree theory taken from ref. [27]. In a comparison of the incoherent-scattering function of C and Fe, all of the previous measurements that the authors searched are shown; previous measurements using a scintillation detector are not shown in the Al, Cu, Pb comparison. No previous measurements of the incoherent-scattering function of Au were searched.

The incoherent scattering function (S) of C and Al measured in this study agreed with S^{WH} within the estimated error (2.5%). This clearly differs from Dow's measurement of the S of Al, which was systematically smaller than S^{WH}; the difference was as large as 6%.

The incoherent scattering function of Fe measured in this study agreed with S^{WH}. Previous measurements of the S of Fe were made by Singh et al. [37] and Anand et al. [38]. However, it was difficult to evaluate the validity of the theoretical values of the S of Fe based on Singh's and Anand's measurements because Singh's measurement was performed in a large momentum-transfer region ($x > 8$ Å^{-1}), where any decrease in the incoherent-scattering function due to the binding effect was tiny, and the estimated error of Anand's measurement was quite large(up to 50%). While the previously measured S of Cu was smaller than S^{WH} in the $1.2 < x < 3.5$ Å^{-1} region, the S of Cu measured in this study agreed well with S^{WH}.

The incoherent scattering function of Au and Pb measured in this study was systematically smaller than S^{WH}, and the discrepancy was 3 to 4% in the case of Au and 4 to 6% in the case of Pb. A possible reason for this discrepancy is given in the next section. Previous measurement of the incoherent-scattering function of Pb tends to larger than S^{WH} in the $1.2 < x < 3$ Å^{-1} region. The 20- and 25-keV photon scattering by Au and Pb samples and 30-keV photon scattering by a Pb sample were not obtained because of a pile-up noise of L-X rays of Au and Pb, respectively.

V. DISCUSSION

In this section, the comparison of measured incoherent scattering function with theoretical one based on a relativistic impulse approximation (S^{IA}) is discussed to investigate the possible reason for the discrepancy between the measured incoherent scattering function of Au and Pb and S^{WH}. Then comparison of a relativistic impulse approximation with an IPA (Independent Particle Approximation) is mentioned.

S^{IA} was obtained by integrating eq.(8) numerically concerning the scattered photon energy (k). Eq.(8) contains the Compton profile of each subshell ($J_i(p_z)$). The tabulated values of $J_i(p_z)$ calculated using Hartree-Fock wave functions ($1 \leq Z \leq 36$) and relativistic Dirac-Hartree-Fock wave functions ($36 \leq Z \leq 102$) by Biggs et al. [34] was used for the integration.

$$S^{IA}(k_0, \theta, Z) = \left\{ \sum_i N_i \int_0^{k_i^{max}} \left(\frac{d^2\sigma}{d\Omega dk}\right)_i dk \right\} \Big/ \left(\frac{d\sigma}{d\Omega}\right)_{fC}, \tag{13}$$

where

$$k_i^{max} = k_0 - I_i. \tag{14}$$

Here, I_i is the binding energy of an electron in the i-th subshell.

In fig.7, comparisons of S^{IA} and S^{WH} with the measurement of S are given for various combinations of k_0 and θ, while maintaining $x = 2.281$ Å^{-1}. The incident energy (k_0) is shown in the upper axis of fig.7. For example, k_0= 28.28 and 500 keV correspond to $\theta = 180°$ and 6.48°, respectively.

The S^{IA} and S^{WH} of Al and Fe agree with each other within a few percent, respectively, and the measured incoherent-scattering function of Al and Fe agrees with them within the experimental error. The measured incoherent scattering function of C and Cu (not shown) also agrees both with S^{WH} and S^{IA} of C and Cu, respectively, within the experimental error. The measured incoherent-scattering function of Au and Pb agrees with S^{IA} and is smaller than S^{WH}. S^{IA} for high-Z atoms (Au and Pb) is clearly dependent of k_0.

Bloch and Mendelsohn [39] performed a calculation of the L-shell Compton profiles and the L-shell incoherent-scattering function using an exact hydrogenic wave function. Bloch and Mendelsohn pointed out that in the case that S^{WH} differs from the exact calculation, S^{IA} is a better approximation to the exact calculation. The present measurement shows the similar tendency concerning the whole-atom incoherent-scattering function.

Recently impulse approximation in bound Compton scattering has been investigated from the point of view of exact independent particle approximation (IPA) [40,41]. The IPA calculation is now limited to K and L electrons only. In the IPA, Compton scattered photon consist of,

(a) Broad Compton peak.

(b) Resonant behavior near characteristic x-ray energies.

(c) Divergence behavior for soft outgoing photons.

Here, (a) corresponds to the energy region of the ordinary Compton scattered photon, (b) and (c) are the low energy part of Compton scattered photon. Relativistic impulse approximation (RIA) agrees well with broad Compton peak of IPA [40]. According to this category, the present measurement is limited to the scattered photon energy region corresponding to (a) *i.e.* Broad Compton peak part. As the present measurement agreed with RIA, it is supposed to agree with (a) of a whole atom IPA calculation when it becomes possible. In the present measurement, scattered photon was not measured in scattered photon energy region corresponding to (b) and (c) due to low detector efficiency under a few keV (Fig.2) and Ge x-ray escape peak (Fig.4). The Compton scattered photon in region (b) and (c) should be examined in the future measurements.

VI. SUMMARY

The incoherent scattering function of C, Al, Fe, Cu, Au, Pb was measured in the $1.14 < x < 2.28$ Å^{-1} region using monochronized synchrotron radiation.

1. The incoherent scattering function (S) of C and Al measured in this study agreed with both S^{WH} and S^{IA} within the estimated error (2.5%). This clearly differs from Dow's measurement of the S of Al, which was systematically smaller than S^{WH}; the difference was as large as 6%.

2. The incoherent scattering function of Fe measured in this study agreed with both S^{WH} and S^{IA}. The present measurement of S of Fe is more precise comparing to previous measurements [37,38].

3. The measured incoherent-scattering function of Cu agrees with both S^{WH} and S^{IA}. This differs from Dow's and Goncalves's measurement of the S of Cu, which was smaller than S^{WH} in the $1.2 < x < 3.5$ Å^{-1} region.

4. The incoherent scattering function of Au was measured for the first time. The measured S of Au agrees with S^{IA} and was smaller than S^{WH} by 3 to 4 %.

5. The measured incoherent scattering function of Pb agrees with S^{IA}, while it is smaller than S^{WH} by 4 to 6%. This differs from Dow's and Kane's measurements of the S of Pb, which tend to be higher than S^{WH} in $x \leq 5$ Å^{-1} region.

ACKNOWLEDGEMENT

The authors express special thanks to N. Watanabe (KEK-PF) for his help as a beam-line manager. Part of the calculation for the data analysis was performed using computers maintained by the Computer Center of KEK.

---

[1] O. Klein and Y. Nishina, Z. Phys. **52**, 853(1929).
[2] I. Waller and D. R. Hartree , Proc. R. Soc. London, Ser. A **124**, 119 (1929).
[3] Y. Namito and H. Hirayama, "Improvement of low energy photon transport calculation by EGS4, Electron Bound Effect in Compton Scattering", Japan Atomic Energy Society, Osaka, March (1991).
[4] A. Samili and C. Depeursinge, "Adaptation du code EGS: Implémentation de l'effet de liaison des électrons lors d'une diffusion Compton", Swiss Federal Institute of Technology, March (1991).
[5] H. M. Colbert, "SANDYL A Computer Program for Calculating Combined Photon-Electron Transport in Complex Systems", SLL-74-0012, Sandia National Laboratory (1974).
[6] Los Alamos Monte Carlo Group, "MCNP-A General purpose Monte Carlo Code for Neutron and Photon Transport", LA-739-M, (Rev.) Ver.2B, LANL (1981).
[7] F. Cleri, Nucl. Instrum. and Meth. **A295**, 231 (1990).
[8] B. S. Sharma and A. N. Tripathi, J. Phys. B: At. Mol. Phys. **13**, 2947 (1980).
[9] R. Ribberfors and K. -F. Berggren, Phys. Rev. A **26**, 3325 (1982).
[10] J. C. Dow, J. P. Lestone, R. B. Taylor and I. B. Whittingham, J. Phys. B: At. Mol. Phys. **21**, 2425 (1988).

[11] P. P. Kane, G. Basavaraju, J. Mahajani and A. K. Priyadarsini, Nucl. Instrum. and Meth. **155**, 467 (1978).
[12] P. P. Kane, J. Mahajani, G. Basavaraju and A. K. Priyadarsini, Phys. Rev. A **28**, 1509 (1983).
[13] O. Goncalves, M. Gaspar and S. de Barros and J. Eichler Phys. Rev. A **30**, 1509 (1984).
[14] R. Quivy, Nucl. Phys. **76**, 362 (1966).
[15] B. Sinha, S. C. Roy and N. Chaudhuri, J. Phys. B: At. Mol. Phys. **9**, 3185 (1976).
[16] S. K. Sen Gupta, N. C. Paul, S. C. Roy and N. Chaudhuri, J. Phys. B: At. Mol. Phys. **12**, 1211 (1979).
[17] S. S. Gopal and B. Sanjeevaiah, J. Phys. B: At. Mol. Phys. **13**, 273 (1980).
[18] S. K. Sen Gupta, N. C. Paul, J. Bose, S. C. Das and N. Chaudhuri, Nucl. Instrum. and Meth. **193**, 395 (1982).
[19] V. V. Rao and D. V. Rao, Phys. Rev. A **28**, 1527 (1983).
[20] A. Bose and A. K. Chatterjee, J. Phys. B: At. Mol. Phys. **20**, 1749 (1987).
[21] D. V. Rao, Appl. Radiat. Isot. **42**, 855 (1991).
[22] W. Phillips and R. J. Weiss, Phys. Rev. **171**, 790 (1968).
[23] T. Paakkari and P. Suortti, Phys. Rev. B **9**, 1756 (1974).
[24] C. B. Walker, Phys. Rev. **103**, 558 (1956).
[25] J. C. R. Laval, Acad. Sci. **215**, 278 (1942).
[26] S. Kahane, J. Phys. B: At. Mol. Opt. Phys. **23**, 1389 (1990).
[27] J. H. Hubbell, W. J. Veigele, E. A. Briggs, R. T. Brown, D. T. Cromer and R. J. Howerton, J. Phys. Chem. Ref. Data **4**, 471 (1975).
[28] P. P. Kane, Phys. Rep. **218**, 67 (1992).
[29] H. Nakashima, S. Tanaka, M. Yoshizawa, H. Hirayama, S. Ban, Y. Namito and N. Nariyama, Nucl. Instrum. and Meth. **A310**, 696 (1991).
[30] W. R. Nelson, H. Hirayama, and D. W. O. Rogers, SLAC-265 (Stanford University, Stanford 1985).
[31] Y. Namito, S. Ban and H. Hirayama, Nucl. Instrum. and Meth. **A332**, 277 (1993).
[32] Y. Namito, S. Ban and H. Hirayama, Nucl. Instrum. and Meth. **A349**, 489 (1994).
[33] RSIC Data Package DLC-136/PHOTOX.
[34] F. Biggs, L. B. Mendelsohn and J. B. Mann, At. Data Nucl. Data Tables **16**, 201 (1975).
[35] R. Ribberfors, Phys. Rev. B **12**, 2067 (1975).
[36] R. Ribberfors, Phys. Rev. A **27**, 3061 (1983).
[37] M. Singh, S. Anand and B. S. Sood, Indian J. Pure Appl. Phys. **1**, 305 (1963).
[38] S. Anand, M. Singh and B. S. Sood, Curr. Sci. **33**, 139 (1964).
[39] B. J. Bloch and L. B. Mendelsohn, Phys. Rev. A **9**, 129 (1974).
[40] P. M. Bergstrom, Jr., T. Surić, K. Pisk, R. H. Pratt, Phys. Rev. A **48**, 1134 (1993).
[41] T. Surić, Nucl. Instrum. and Meth. **A314**, 240 (1992).

TABLE I. Thicknesses of the samples.

Sample Thickness (g/cm^2)					
C	Al	Fe	Cu	Au	Pb
0.1325	0.2711	1.57	1.79	3.86	0.568

TABLE II. Estimated sources of errors.

Errors	Magnitude (%)	Errors	Magnitude (%)
μ_t	1.5	Solid angle of Collimators	0.5
Monitor	1.0	Fitting	0.5
Orientation of Sample	1.0	Statistics of Measurement	<0.5
Ge efficiency	1.0	Statistics of MS Calculation	<0.5
		Total	2.5

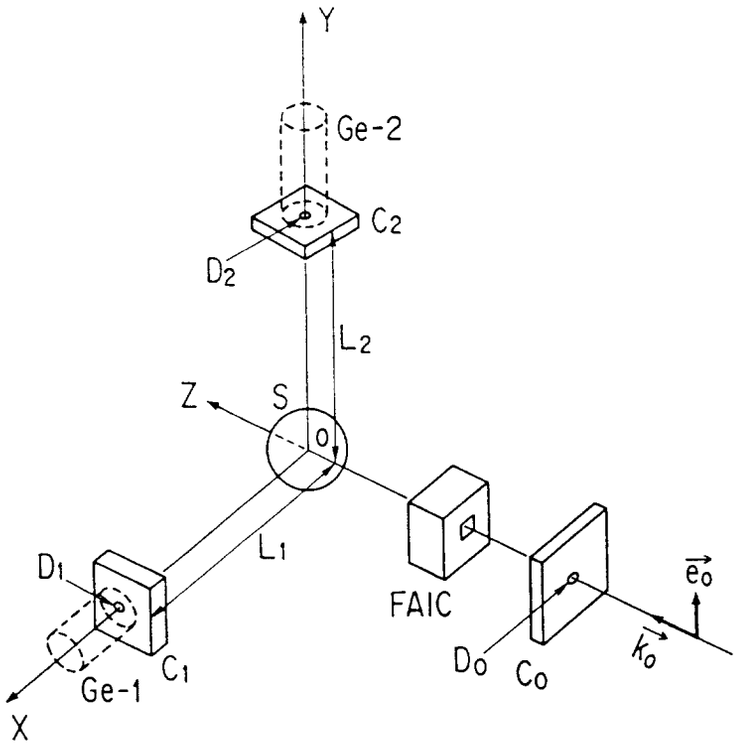

FIG. 1. Experimental arrangement. The incident photon beam passed through a collimator (C_0) with an opening diameter (D_0) of 2 mm and a free air ionization chamber (FAIC), and scattered by a sample (S) located at point O. The normal vector of the sample was ($-\frac{1}{2}, -\frac{1}{\sqrt{2}}, \frac{1}{2}$). Photons passing through collimators located in the X and Y directions (C_1 and C_2) were detected by Ge detectors (*Ge*-1 and *Ge*-2, respectively). The distances from the surface of the sample to the exit of the collimator (L_1 and L_2) were 424 and 436 mm and opening diameters of the collimators (D_1 and D_2) were 5.01 and 5.04 mm.

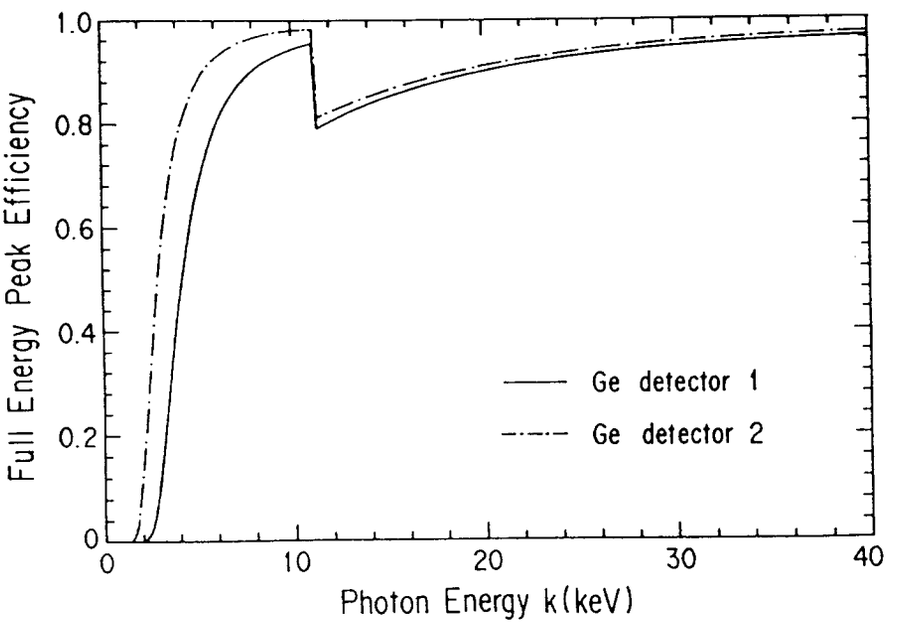

FIG. 2. Full-energy peak efficiency of the Ge detector 1 and 2.

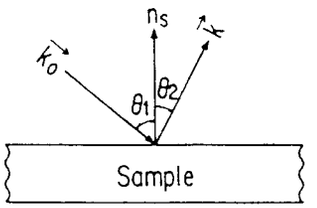

FIG. 3. Scattering of a photon by a plane sample.

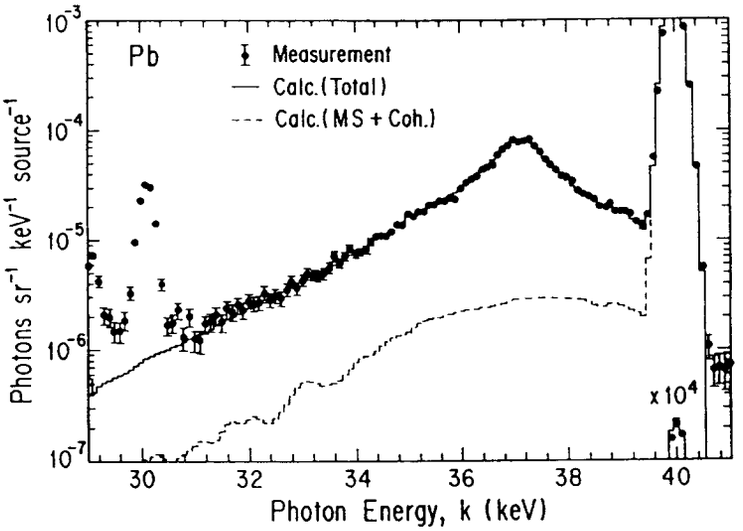

FIG. 4. Scattered-photon spectrum from a Pb sample (k_0 = 40 keV). The measured and calculated values are indicated by symbols and histograms, respectively. The sharp peak at 30 keV is the Ge K X-ray escape peak of the Rayleigh-scattering peak at 40 keV. The broad peak at 37 keV is the Compton-scattering peak.

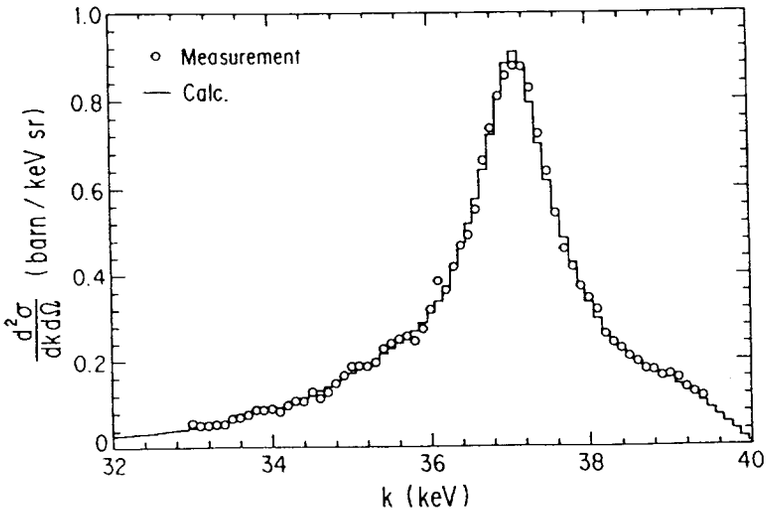

FIG. 5. Comparison of the Gauss-smeared $\frac{d^2\sigma}{d\Omega dk}(\phi = \frac{\pi}{4})$ with the measurement. The sample was Pb; k_0=40keV and $\theta = 90°$.

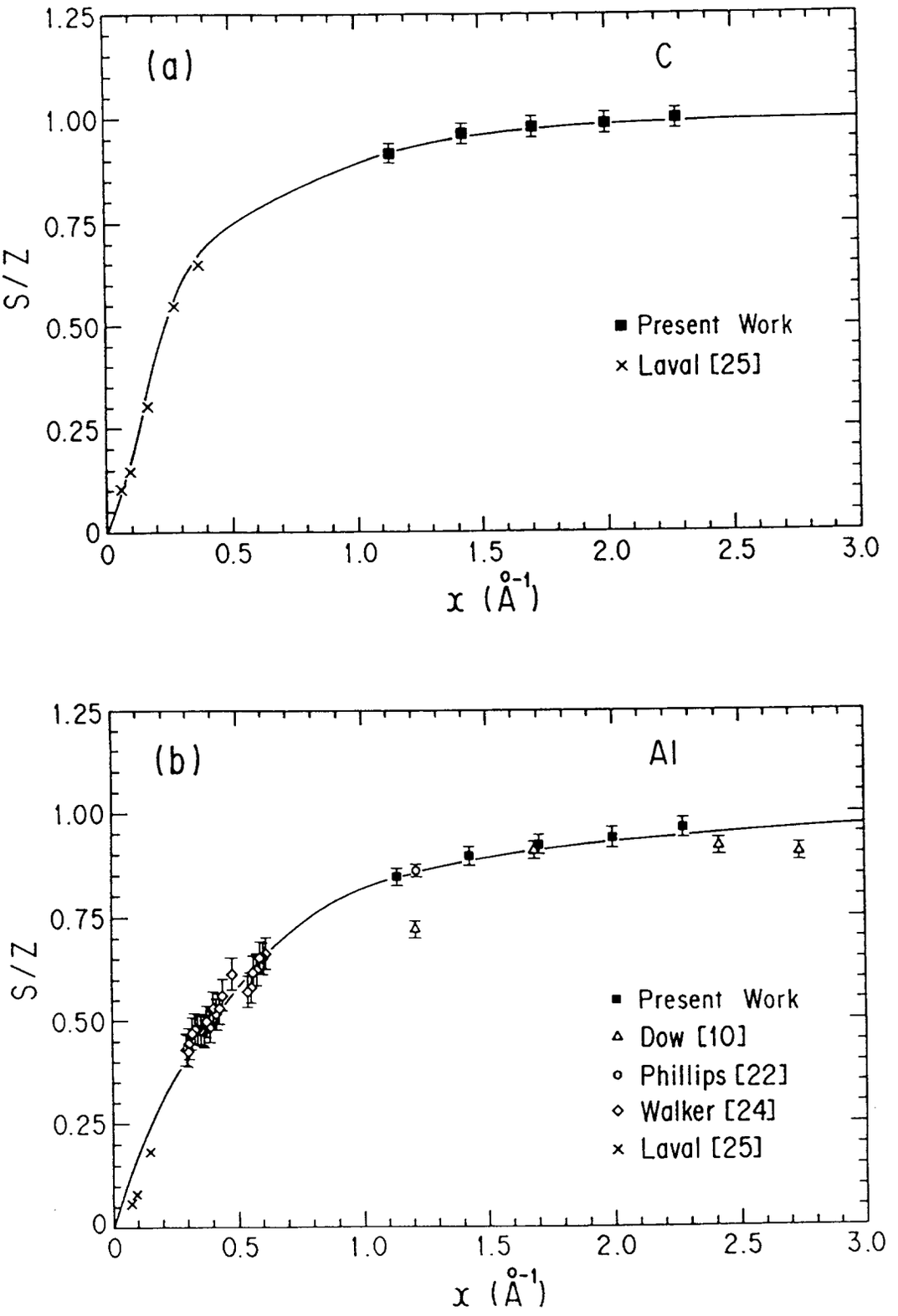

FIG. 6. Incoherent scattering function.

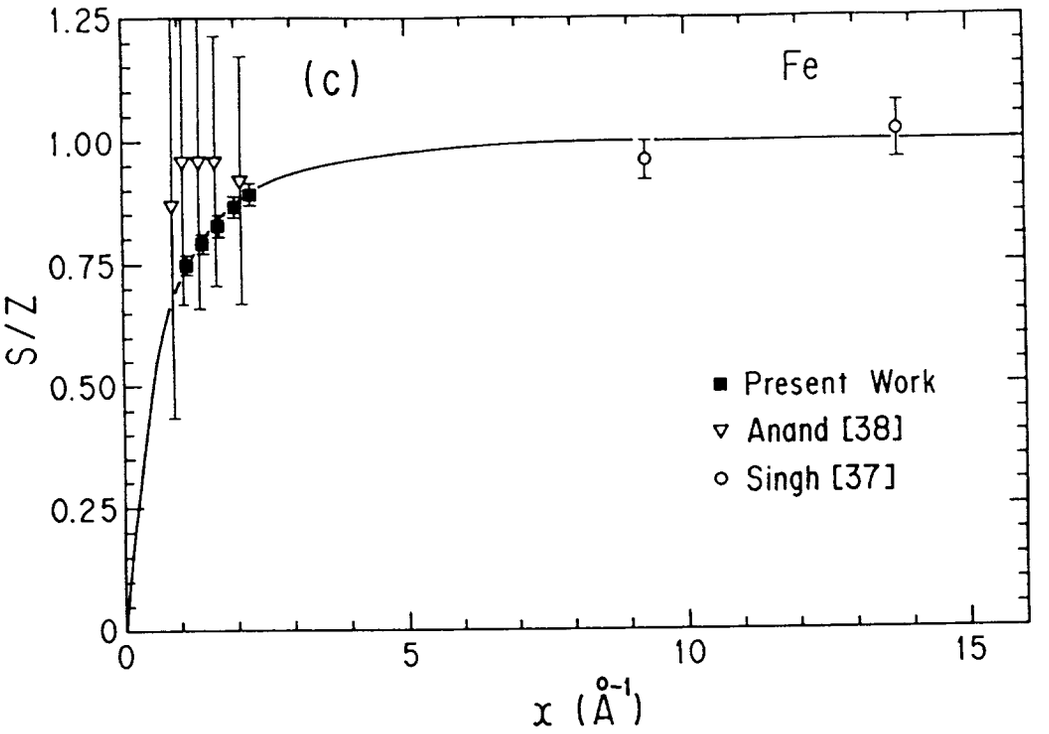
(c)
Fe
S/Z
x (Å^{-1})
Present Work
Anand [38]
Singh [37]

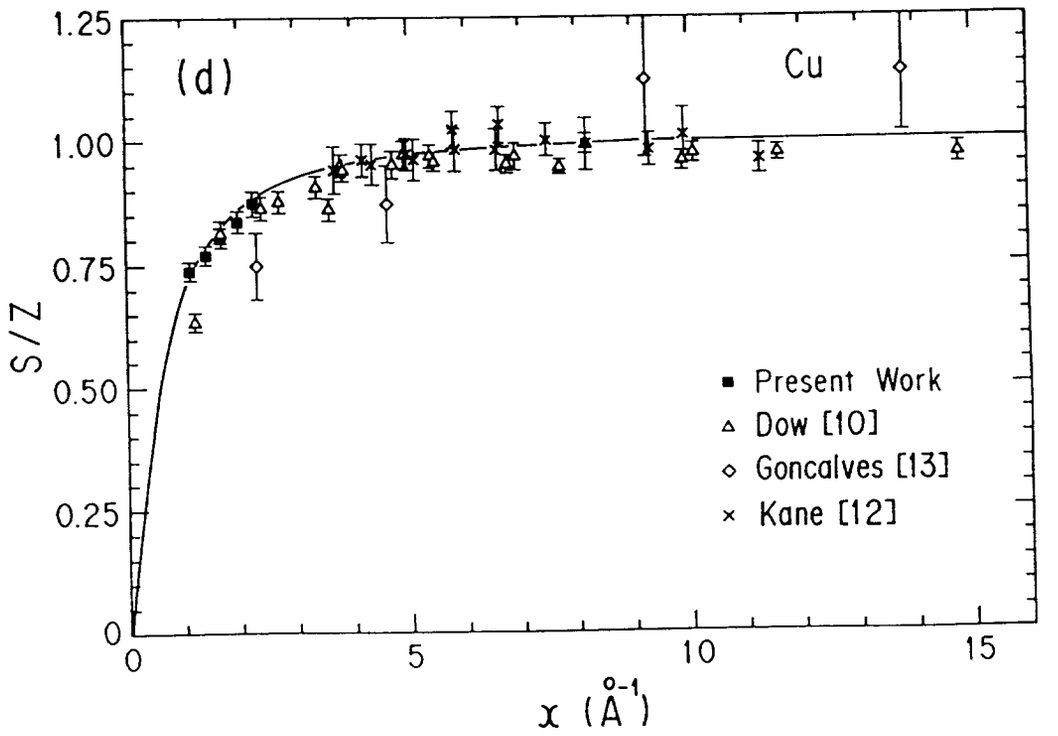
(d)
Cu
S/Z
x (Å^{-1})
Present Work
Dow [10]
Goncalves [13]
Kane [12]

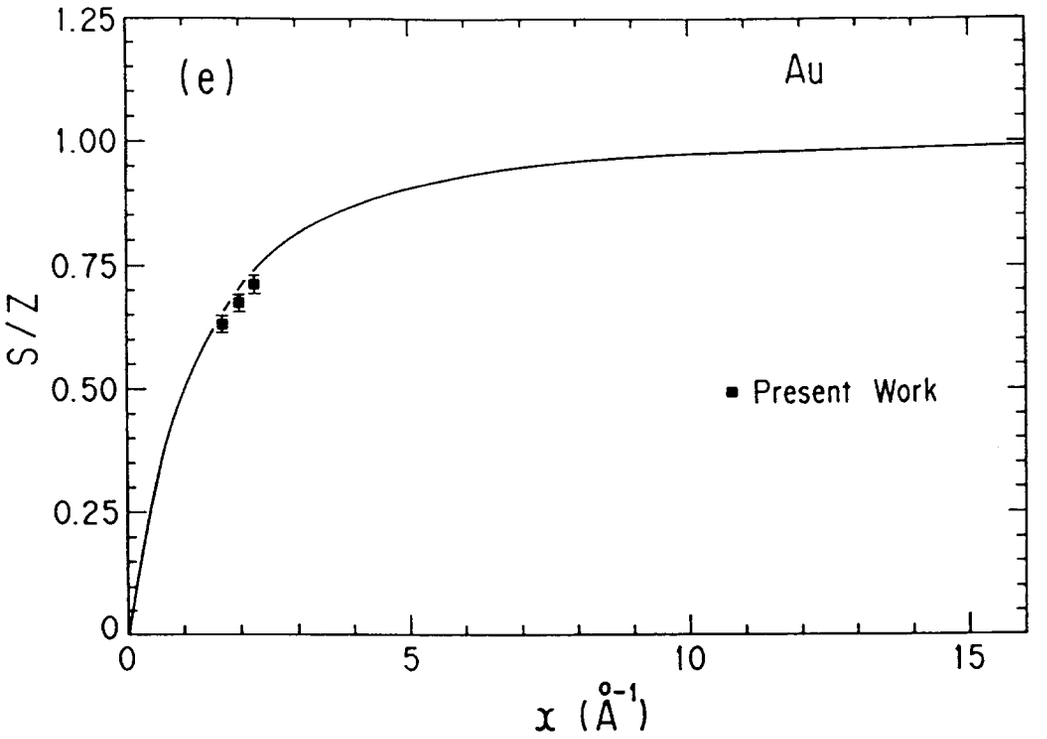
(e)
Au
1.25
1.00
0.75
0.50
0.25
0
S/Z
0
5
10
15
x (Å^{-1})
Present Work

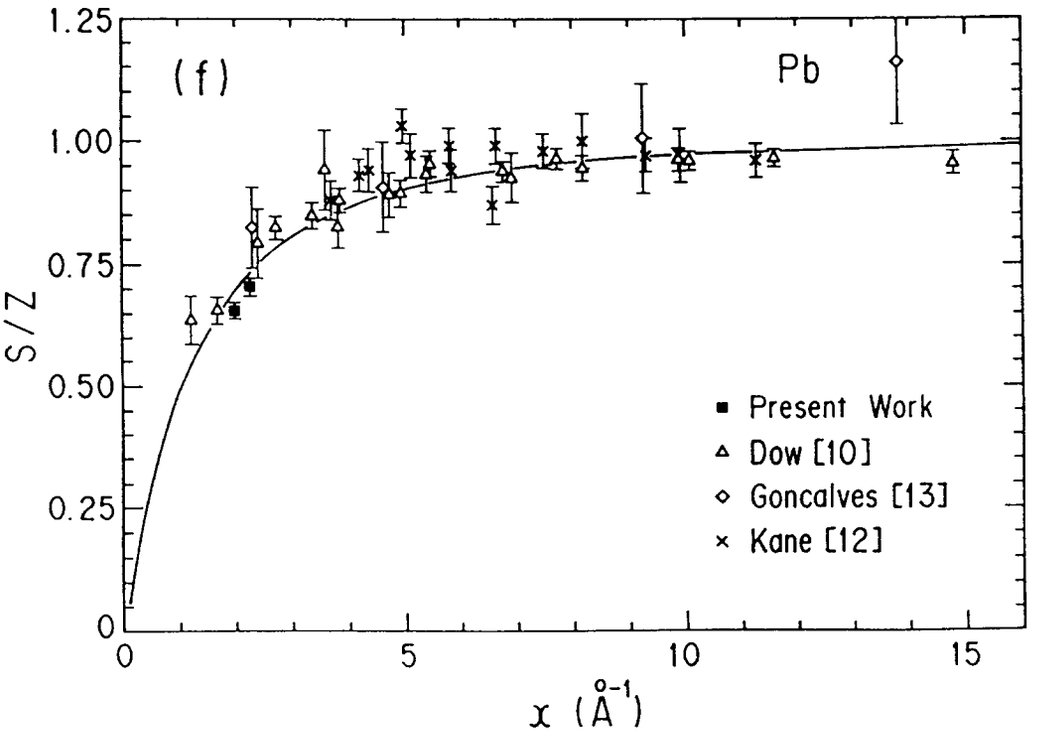
(f)
Pb
1.25
1.00
0.75
0.50
0.25
0
S/Z
0
5
10
15
x (Å^{-1})
Present Work
Dow [10]
Goncalves [13]
Kane [12]

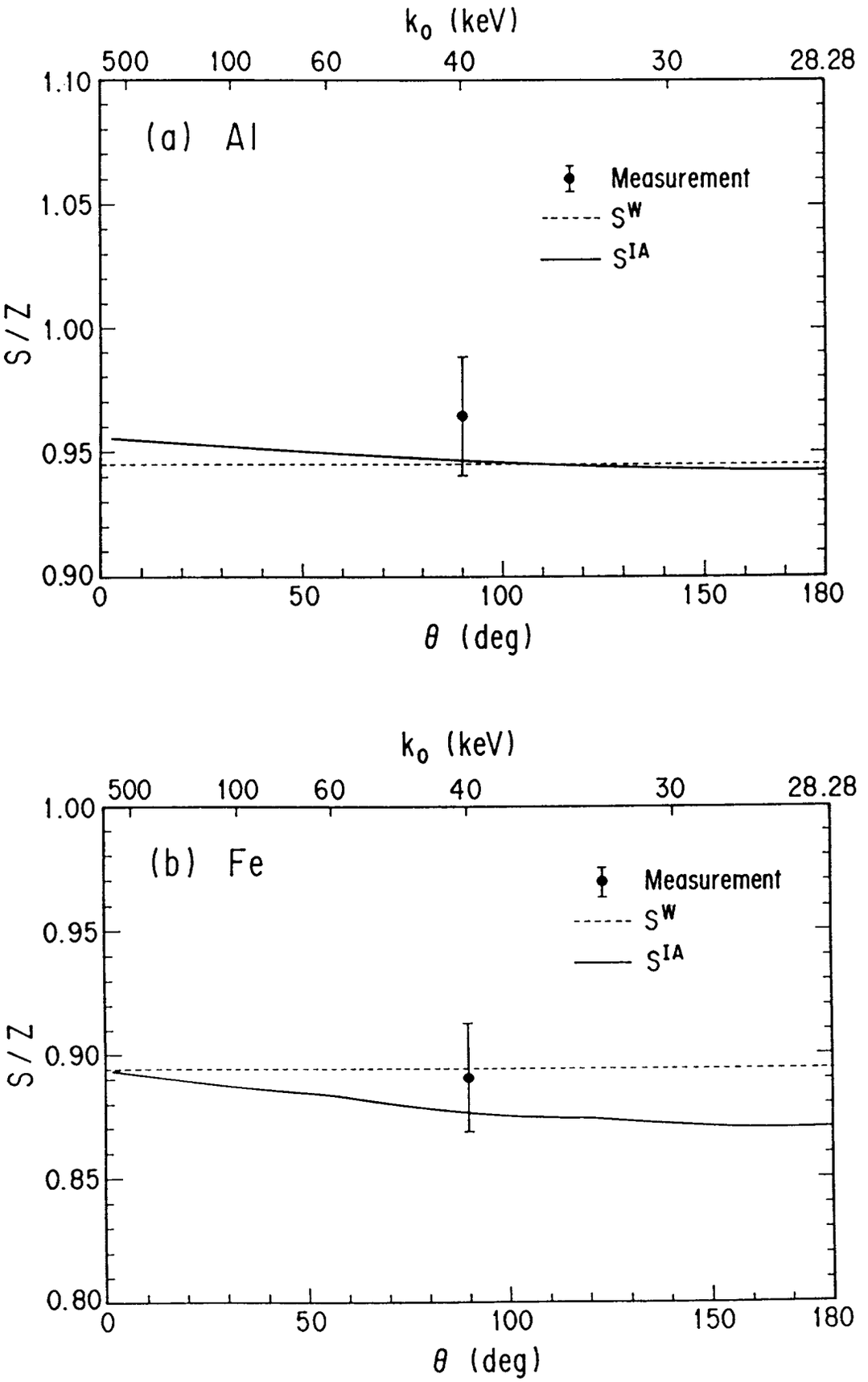

FIG. 7. Comparison of S for different θ and k_0 (x=2.281 Å^{-1}).

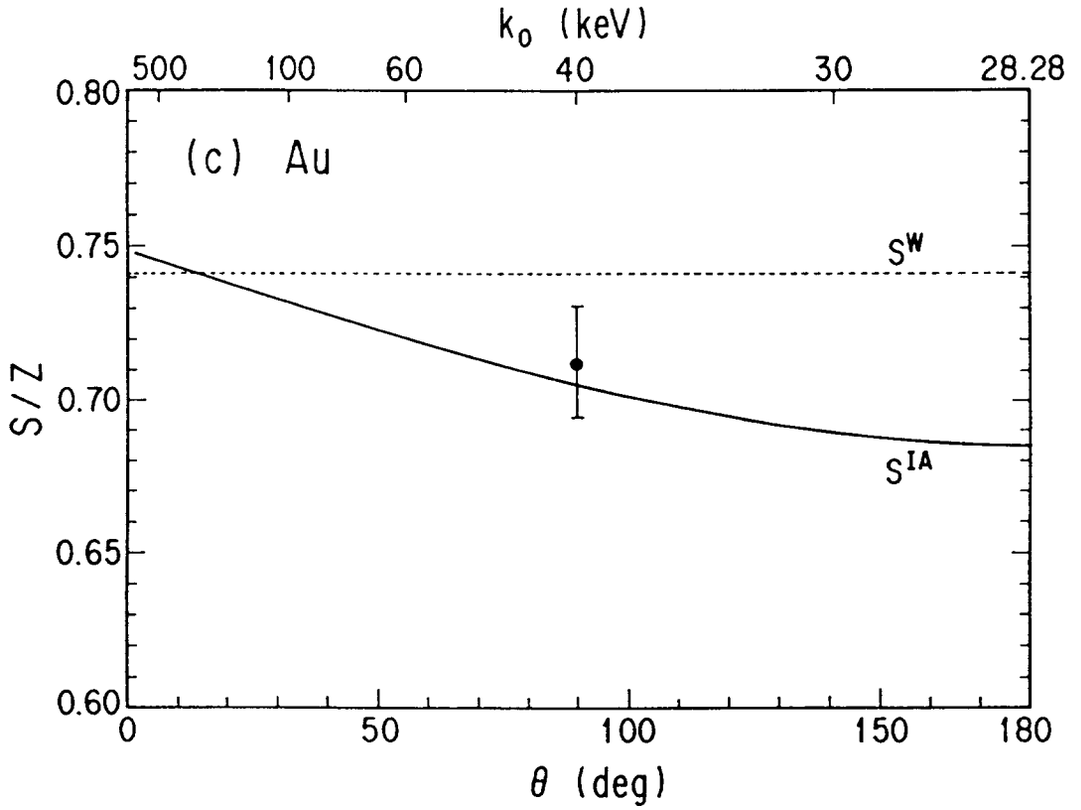
k0 (keV)
500
100
60
40
30
28.28
0.80
0.75
0.70
0.65
0.60
(c) Au
S^W
S^IA
S / Z
0
50
100
150
180
θ (deg)

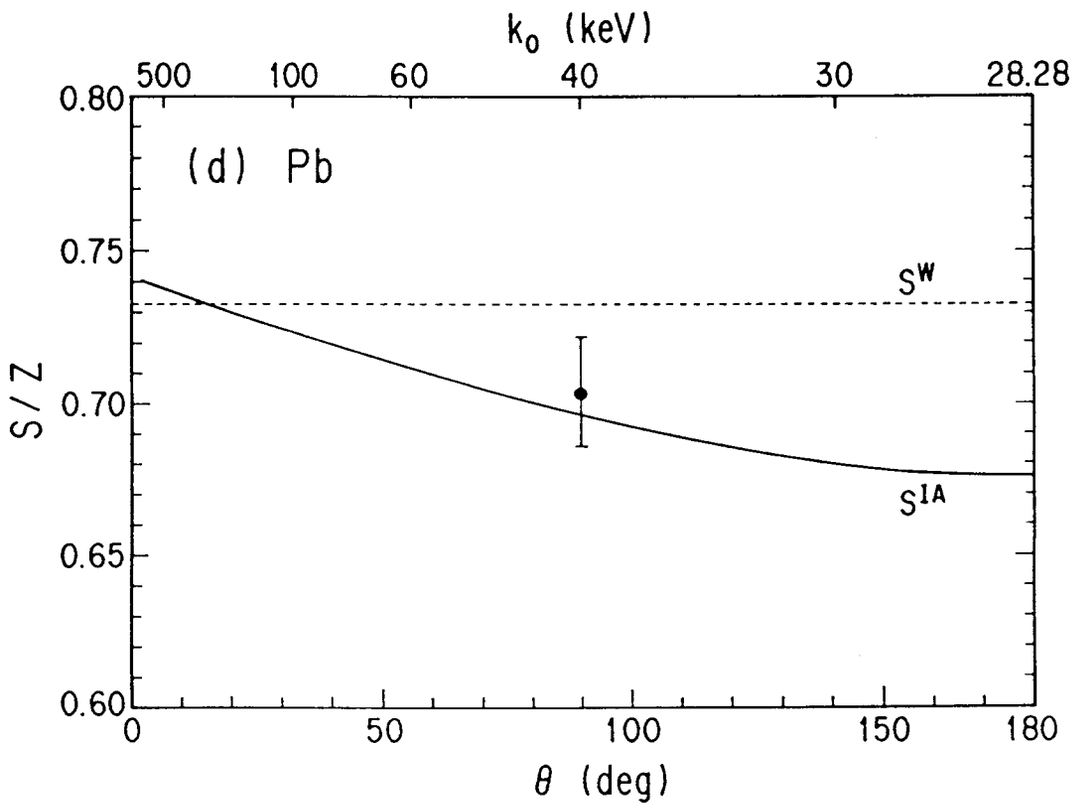
k0 (keV)
500
100
60
40
30
28.28
0.80
0.75
0.70
0.65
0.60
(d) Pb
S^W
S^IA
S / Z
0
50
100
150
180
θ (deg)